Electronic Supplementary Information (ESI)

for

Selective H_2O_2 conversion to hydroxyl radicals in electron-rich area of hydroxylated C-g-C_3N_4/CuCo-Al_2O_3

Lai Lyu[ab], Lili Zhang[a], Guangzhi He[c], Hong He[bc] and Chun Hu[*,ab]*

[a]Key Laboratory of Drinking Water Science and Technology, Research Center for Eco-Environmental Sciences, Chinese Academy of Sciences, Beijing 100085, China.

[b]University of Chinese Academy of Sciences, Beijing 100049, China.

[c]State Key Joint Laboratory of Environment Simulation and Pollution Control, Research Center for Eco-Environmental Sciences, Chinese Academy of Sciences, Beijing 100085, China

*Tel: +86-10-62849628; fax: +86-10-62923541; e-mail: huchun@rcees.ac.cn

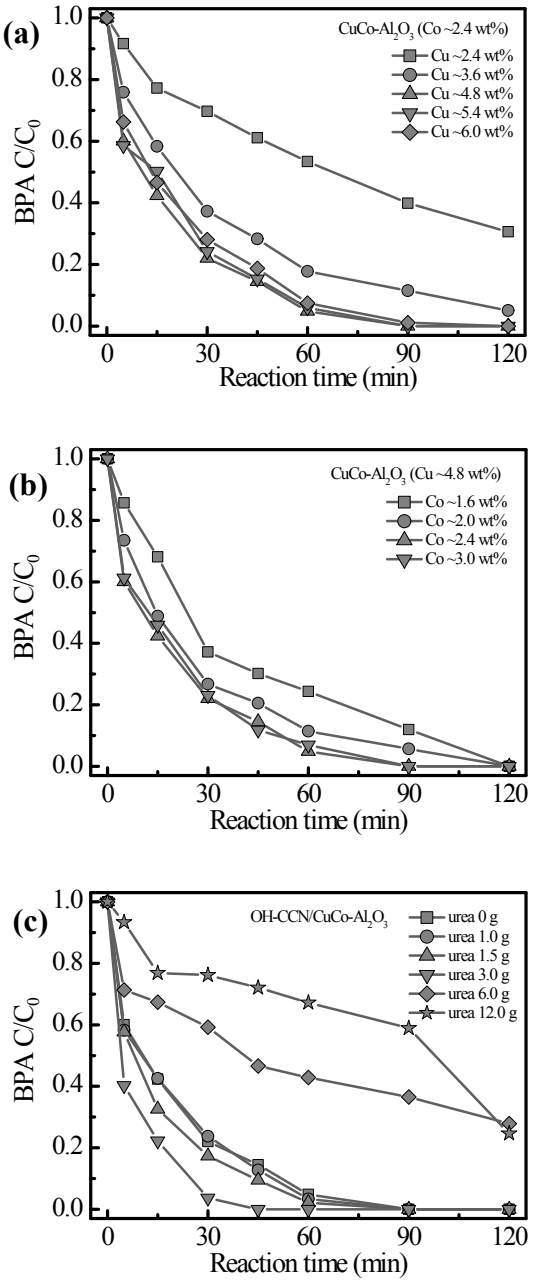

Figure S1. Effect of the amount of the introduced (**a**) Cu and (**b**) Co in CuCo-Al_2O_3 and (**c**) the used urea during the preparation of OH-CCN/CuCo-Al_2O_3 on BPA degradation with H_2O_2 (Initial pH 7, initial BPA concentration 25 mg L^{-1}, initial H_2O_2 concentration 10 mM, catalyst 0.8 g L^{-1}).

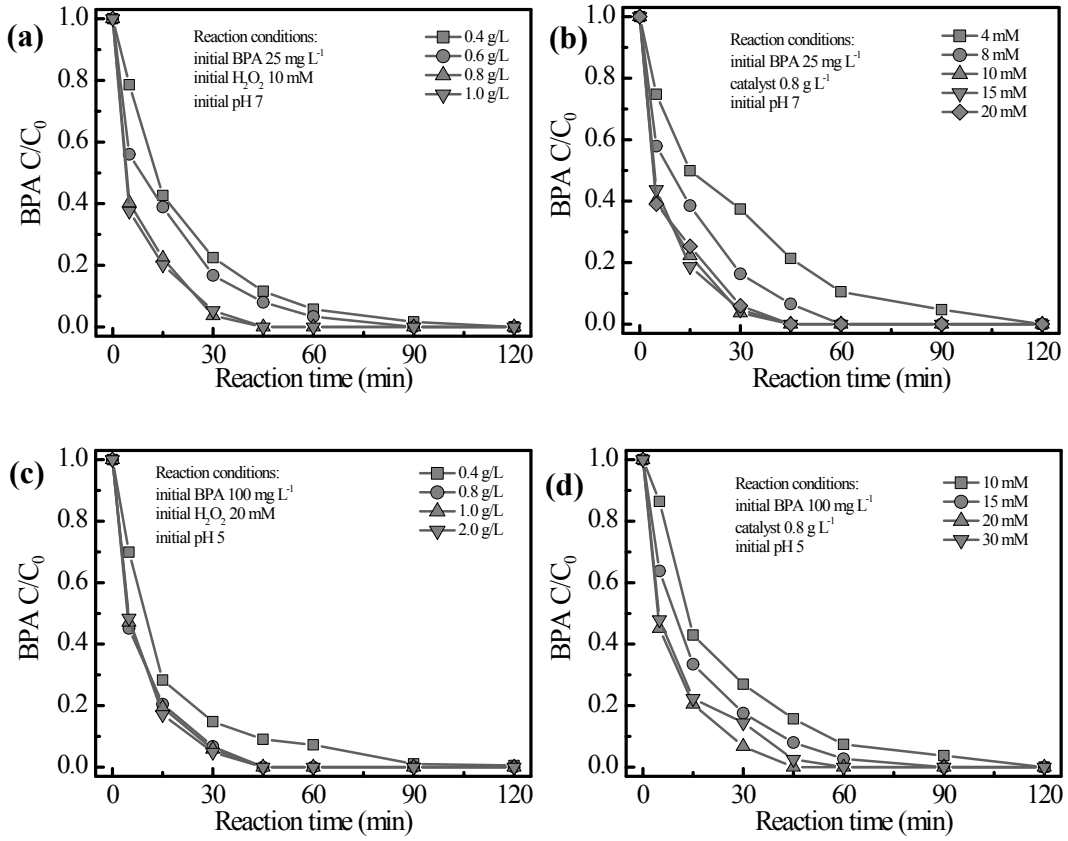

Figure S2. Effect of (**a**) catalyst concentration and (**b**) H_2O_2 dosage on 25 mg L^{-1} BPA degradation in the OH-CCN/CuCo-Al_2O_3 suspension at pH 7; and effect of (**c**) catalyst concentration and (**d**) H_2O_2 dosage on 100 mg L^{-1} BPA degradation in the OH-CCN/CuCo-Al_2O_3 suspension at pH 5.

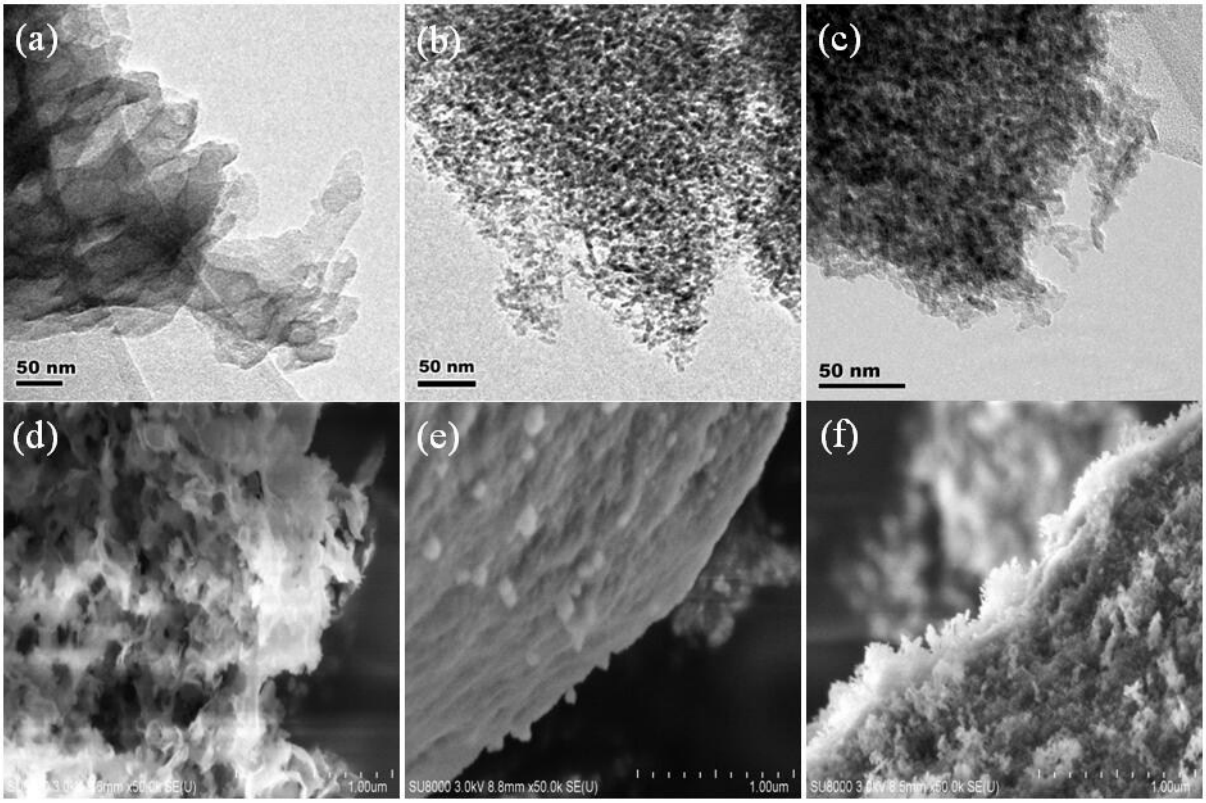

Figure S3. TEM of (a) g-C_3N_4, (b) CuCo-Al_2O_3 and (c) OH-CCN/CuCo-Al_2O_3. SEM of (d) g-C_3N_4, (e) CuCo-Al_2O_3 and (f) OH-CCN/CuCo-Al_2O_3.

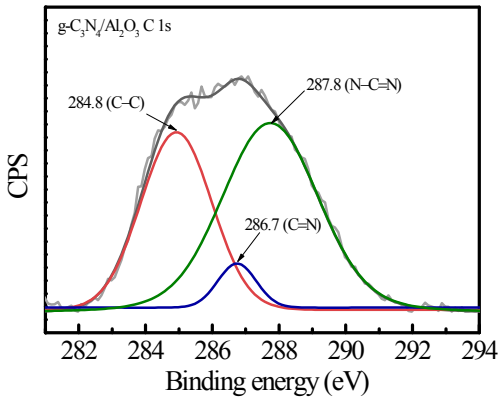

Figure S4. XPS spectra in C 1s for g-C_3N_4/Al_2O_3.

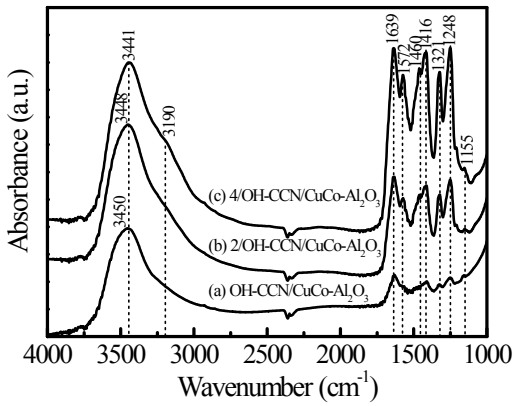

Figure S5. FTIR spectra for OH-CCN/CuCo-Al_2O_3 with different amount of g-C_3N_4: (a) normal OH-CCN/CuCo-Al_2O_3, (b) OH-CCN/CuCo-Al_2O_3 with 2 times of g-C_3N_4 (2/OH-CCN/CuCo-Al_2O_3) and (c) OH-CCN/CuCo-Al_2O_3 with 4 times of g-C_3N_4 (4/OH-CCN/CuCo-Al_2O_3).

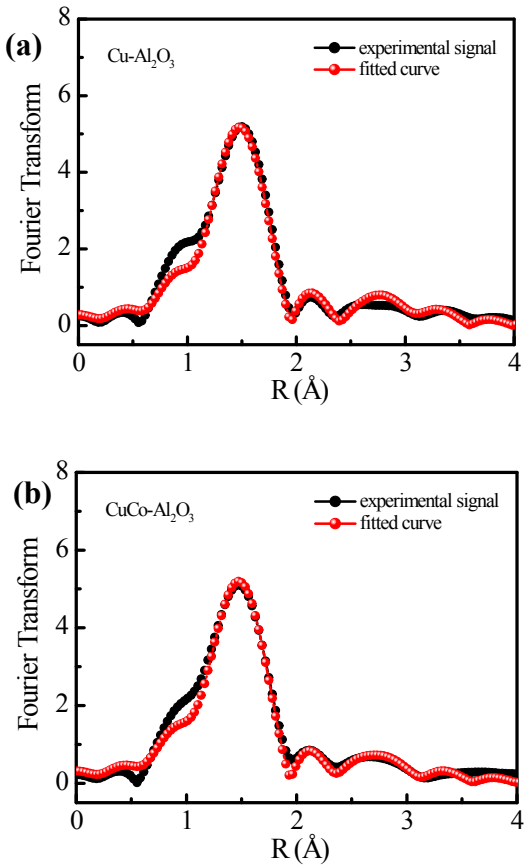

Figure S6. The EXAFS curve fitting for Cu K-edge of (**a**) Cu-Al_2O_3 and (**b**) CuCo-Al_2O_3. (solid line–experimental signals, dotted line–fitted curves).

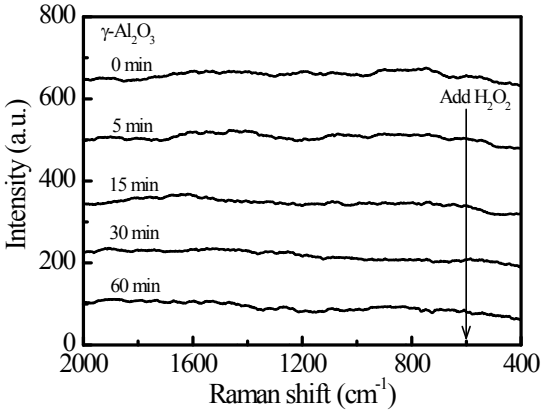

Figure S7. *In situ* Raman spectra of γ-Al_2O_3 aqueous dispersion recorded at different time after adding H_2O_2.

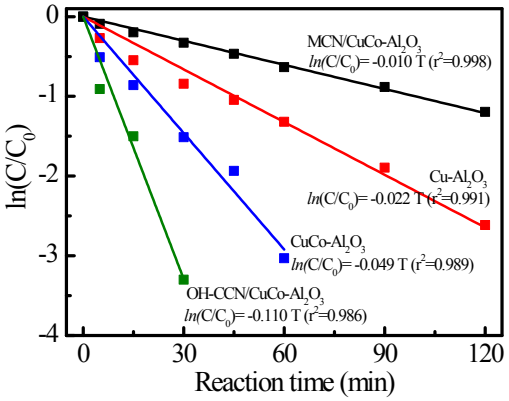

Figure S8. Kinetic curves of BPA degradation in various suspensions (Initial pH 7, initial BPA 0.1 mM, initial H_2O_2 10 mM, catalyst 0.8 g L^{-1}).

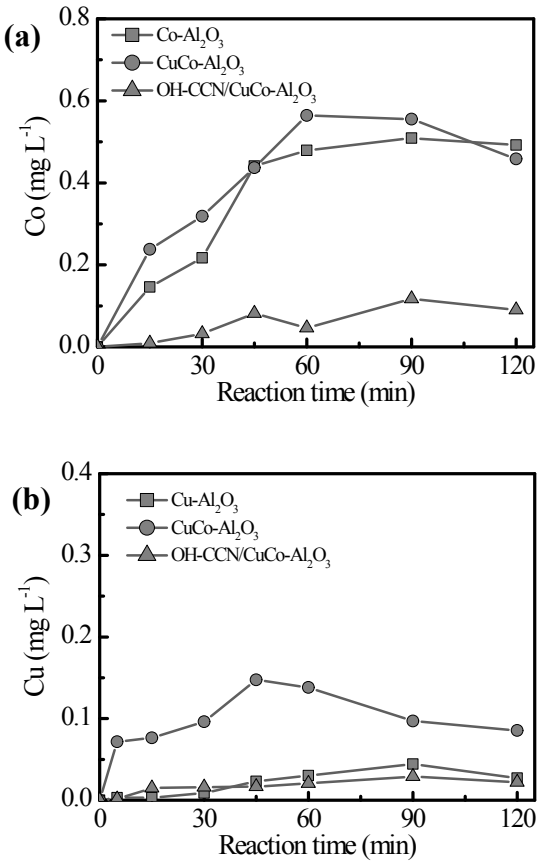

Figure S9. Release of (**a**) Co and (**b**) Cu in Co-Al_2O_3, Cu-Al_2O_3, CuCo-Al_2O_3 and OH-CCN/CuCo-Al_2O_3 suspensions during the reaction with H_2O_2. Zero point (0 min) has been calibrated by deducting the metal ion release from the catalyst before adding H_2O_2.

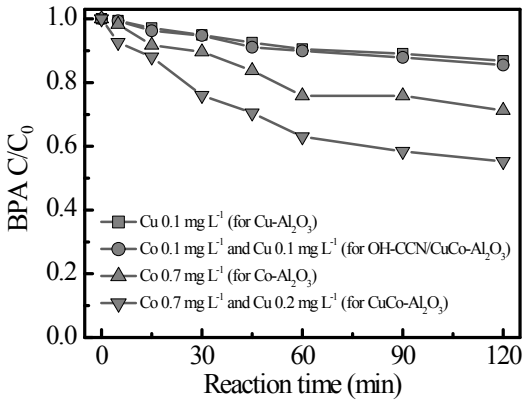

Figure S10. Homogeneous Fenton degradation of BPA in various suspensions (Initial BPA 0.1 mM, initial H_2O_2 10 mM).

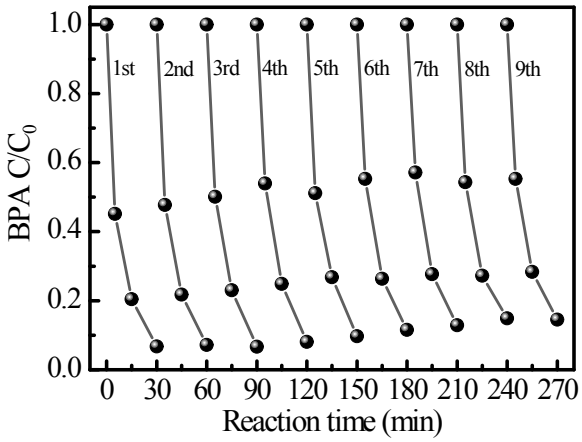

Figure S11. Cycling runs for the degradation of BPA in the OH-CCN/CuCo-Al_2O_3 suspension (Initial pH 7, initial BPA 0.1 mM, initial H_2O_2 10 mM, catalyst 0.8 g L^{-1}).

Table S1. BET surface area, pore diameter, pore volume and metal content information of the various samples.

Samples	BET surface area ($m^2 g^{-1}$)	Pore diameter (nm)	Pore volume ($cm^3 g^{-1}$)	Cu content (wt%)	Co content (wt%)
γ-Al_2O_3	270.7	5.5	0.48	0	0
Cu-Al_2O_3	222.0	6.3	0.45	4.79	0
CuCo-Al_2O_3	186.0	8.5	0.48	4.82	2.45
OH-CCN/CuCo-Al_2O_3	188.8	8.2	0.47	4.81	2.43

Table S2. EPR-measured g and A values for Cu(II) species in various samples.

Samples	$g_{//}$	$g_{\perp}$	$A_{//}$ (G)
Cu-Al_2O_3	2.3862	2.1333	150
CuCo-Al_2O_3	2.3825	2.1163	150
OH-CCN/CuCo-Al_2O_3	2.3751	2.0995	150
2/OH-CCN/CuCo-Al_2O_3	2.3665	2.0990	150
4/OH-CCN/CuCo-Al_2O_3	2.3630	2.0985	150

Table S3. Actual H_2O_2 consumption ($[\Delta H_2O_2]_A$) and stoichiometric H_2O_2 consumption ($[\Delta H_2O_2]_S$) for mineralizing the pollutants during the reaction.

(a) $[\Delta H_2O_2]_A$, $[\Delta H_2O_2]_S$ and $\eta[H_2O_2]$ for mineralizing equivalent BPA in different catalyst suspensions.

entry	catalyst[a]	time (min)	TOC removal (mg L^{-1})	$[\Delta H_2O_2]_A$ (mM)	$[\Delta H_2O_2]_S$ (mM)	$\eta[H_2O_2]$ (%)
1	Cu-Al_2O_3	120	72.1%	3.51	2.86	81.5
2	CuCo-Al_2O_3	120	75.1%	3.77	2.97	78.8
3	OH-CCN/CuCo-Al_2O_3	60	73.5%	3.23	2.91	90.1

[a]Reaction conditions: initial [BPA] = 25 mg L^{-1}, initial $[H_2O_2]$ = 0.01 mol L^{-1}, [catalyst] = 0.8 g L^{-1}, initial pH=7, 308 K.

(b) $[\Delta H_2O_2]_A$) and $[\Delta H_2O_2]_S$ for mineralizing various pollutants in the OH-CCN/CuCo-Al_2O_3 system.

entry	contaminants[a]	initial conc. (mg L^{-1})	time (min)	$[\Delta H_2O_2]_A$ (mM)	$[\Delta H_2O_2]_S$ (mM)
1	benzene	100	30	9.07	8.57
2	phenol	100	30	12.61	11.72
3	benzoic acid	100	30	3.93	3.63
4	phloroglucinol	100	30	6.04	5.59
5	bisphenol A[b]	25	30	2.91	2.66
6	bisphenol A	100	30	12.12	11.32
7	2-chlorophenol	50	30	2.99	2.76
8	4-isopropylphenol	100	30	8.58	7.89
9	ibuprofen	30	30	2.93	2.67
10	phenytoin	30	30	2.65	2.42
11	diphenhydramine	30	30	3.05	2.76
12	2,4-dichlorophenoxyacetic acid	100	30	3.74	3.45
13	methyl orange	50	30	4.69	4.24
14	rhodamine B	50	30	4.52	4.2
15	methylene blue	80	30	5.44	4.72
16	atrazine	15	30	1.3	1.04

[a]Reaction conditions: initial $[H_2O_2]$ = 0.02 mol L^{-1}, [catalyst] = 0.8 g L^{-1}, initial pH=5, 308 K.

[b]initial $[H_2O_2]$ = 0.01 mol L^{-1}, [catalyst] = 0.8 g L^{-1}, initial pH=7, 308 K.

Table S4. Comparison of the degradation of BPA by heterogeneous Fenton methods.

Entry	Catalyst	BPA Conc. (mM)	H_2O_2 dose (mM)	Conditions	Reaction time (min)	Removal efficiency (%)	Utilization efficiency of H_2O_2(%)	Ref.
1	Fe_3O_4 NPs	0.1	20	pH 5	120	19	5.2	1
2	Cu_2O MPs	0.1	20	pH 5	120	60	19.6	1
3	$CuFeO_2$ MPs	0.1	20	pH 5	120	99.2	57.8	1
4	Fe_3O_4 MNPs	~0.1	160	pH 3 ultrasonic processing	480	100	——	2
5	$BiFeO_3$	0.1	10	pH 5 303 K	120	20.4	——	3
6	OH-CCN/ CuCo-Al_2O_3	**~0.1**	10	ambient conditions (~pH 7)	**30**	**96.3**	**90.5**	This work
7	Au/SRAC	~0.5	~16	pH 3 313 K	720	89	——	4
8	Au/Fe_2O_3	~0.5	~16	pH 3 313 K	720	10.1	——	4
9	Au-Fe_2O_3/Al_2O_3	~0.5	~16	pH 3 313 K	720	6.6	——	4
10	OH-CCN/ CuCo-Al_2O_3	**~0.5**	20	pH 5 308 K	**30**	**93.3**	**93.4**	This work

Supplementary Methods

Characterization of Catalyst

N_2 adsorption-desorption: The Brunner−Emmet−Teller (BET) specific surface area, pore diameter and pore volume were obtained on a gas sorption analyzer (ASAP 2020 HD88) at the temperature of liquid nitrogen. The samples were previously outgassed for 30 min at 150 °C and 4 Pa and then heated for 120 min at 350 °C.

XRD: Powder X-ray diffraction (XRD) patterns were recorded on a Scintag-XDS-2000 diffractometer with Cu Kα radiation (λ = 1.540598 Å) operating at 40 kV and 40 mA. The wide diffraction angle analysis was conducted in a range of 5 to 90° with a scanning speed of 5°/min.

EXAFS: Extended X-ray absorption fine structure (EXAFS) spectra were recorded at the beam lines BL14W1 of the Shanghai Synchrotron Radiation Facility (SSRF), China. Cu foil, Cu_2O and CuO were used as references. The samples were sealed between two layers of adhesive PVC tape. The Cu K-edge (8.979 keV) EXAFS spectra of the samples were collected under ambient conditions in transmission mode. The parameters for EXAFS measurements, data collection modes and error calculations were all controlled according to guidelines set by the International XAFS Society Standards and Criteria Committee. The EXAFS data were analyzed by the Athena program. EXAFS oscillations $\chi(k)$ were extracted using spline smoothing and weighted by k^3 to compensate for the diminishing amplitude in the high k range. The filtered k^3 weighted $\chi(k)$ were Fourier transformed (FT) to R space in the k range of 2 to 11 $Å^{-1}$. A nonlinear least-squares algorithm was applied to the EXAFS fitting with phase correlation in the R space between 1 and 4 Å for the Cu K-edge. The structural parameters of the samples were obtained via curve fitting procedures using the FEFF8.4 code.[5]

XPS: X-ray photoelectron spectroscopy (XPS) data were recorded on an AXIS-Ultra instrument using monochromatic Al Kα radiation (225 W, 15 mA, 15 kV) and low-energy

electron flooding for charge compensation. To compensate for surface charge effects, the binding energies were calibrated using the C1s hydrocarbon peak at 284.80 eV.

FTIR: Fourier-transform infrared spectroscopy (FTIR) was recorded on a Nicolet 8700 FTIR spectrophotometer (Thermo Fisher Scientific Inc., USA) in the range of 4000-400 cm^{-1}. The dry samples were supported on KBr pellets at a fixed proportion (1 wt%). All spectra were measured with a resolution of 4 cm^{-1} and with an accumulation of 32 scans.

Procedures, Analysis and Calculation

Detection of $^{\bullet}OH$ and $O_2^{\bullet-}$ EPR signals: BMPO-trapped EPR signals were detected in different air-saturated methanol/aqueous dispersions of the corresponding samples. Typically, in the absence of H_2O_2, 0.05 g of the prepared powder sample was added to 1 mL of water (for detecting $^{\bullet}OH$) or water/methanol (10%/90%, V/V, for detecting $O_2^{\bullet-}$). 20 μL of BMPO (250 mM) was added and held for 5 min. Then, the solution was sucked into the capillary. The EPR spectra were recorded on a Bruker A300-10/12 EPR spectrometer at room temperature. In the presence of H_2O_2, 0.01 g of the prepared powder sample was added to 1 mL of water (for detecting $^{\bullet}OH$) or methanol (for detecting $O_2^{\bullet-}$). Then, 100 μL of the above suspension, 10 μL of BMPO (250 mM) and 10 μL of H_2O_2 (30%, w/w) were mixed and held for 5 min. The solution was sucked into the capillary to carry out EPR detection.

Measurement of *in situ* Raman spectra: *In situ* Raman spectra of the samples were collected on an inVia-Reflex confocal microscopic Raman spectrometer (Reinishaw, UK) with 40 mW 532 nm laser light irradiation. In a typical procedure, 0.1 g of the prepared powder sample were mixed with 3 mL of water, and the mixture was placed into the reaction cell, which was scanned from 400 to 2000 cm^{-1} at a resolution of 1 cm^{-1} for 120 s on the Raman spectrometer. Then, 50 μL of H_2O_2 (30%, w/w) was added followed by immediate stirring. At given time intervals, the scanning procedure described above was repeated.

Computational methods of density functional theory (DFT): The optimization of geometry and wave function was performed using B3LYP functional[6] and 6-31G(d) basis set with the Gaussian 09 package.[7] The valence-electron density was analyzed with the Multiwfn package.[8] The geometry was visualized using VMD software.[9] The carbon-doped g-C_3N_4 was modeled using a $C_9N_{12}H_6$ planar cluster with one N atom replaced by one C atom. The carbon-doped g-C_3N_4 was complexed with the Cu atom doped in γ-Al_2O_3 by the surface oxygen functional group. The dangling bonds of the O atoms coordinated to Cu in γ-Al_2O_3 were terminated with H atoms to obtain neutral cluster. Due to the size and edge effects, the properties estimated with the finite-size model may vary from those of the real system to some extent. However, it can be expected that the results obtained with the current model would be qualitatively reliable in predicting the local chemical properties.

Quantification of •OH by the TPA probe method: The generation of •OH· in the OH-CCN/CuCo-Al_2O_3 aqueous dispersion was quantitatively measured using the terephthalic acid (TPA) probe method, in which the trapping of •OH by TPA could generate the strongly fluorescent 2-hydroxyl-terephthalic acid (2-HTPA). The TPA solution was prepared with 4 mM of TPA and 12 mM of NaOH mixture. In a typical procedure, 50 mL of the TPA solution and 0.02 g of the catalyst powder were placed in a beaker. The pH value was adjusted to 6-6.5 using the aqueous hydrochloric acid solution. The suspensions were magnetically stirred for 5 min under ambient air conditions. Then, H_2O_2 with different concentrations (1 mM, 2 mM, 5 mM, 10 mM and 20 mM) was added to the suspensions under magnetic stirring throughout the experiment. At given time intervals, 3 mL aliquots were collected and filtered through a Millipore filter (pore size 0.45 μm) to detect the H_2O_2 consumption and the 2-HTPA (•OH) production based on the fluorescence intensity. The fluorescence intensity of the produced 2-HTPA was detected by a CARY ECLIPSE fluorescence spectrophotometer. The excitation and emission wavelengths of the detector were set at 310 and 424 nm, respectively.

Simultaneously, the concentration of H_2O_2 was determined using a DPD method, as previously reported in literature.[10]

Measurement and calculation of TOF: The turnover frequency (TOF) of OH-CCN/CuCo-Al_2O_3 was obtained from the conversion number of H_2O_2 into •OH· per second on one active site. It is well known that the reaction involves free radical chain reactions in solution. As the reaction time increased, the accuracy of the measured value decreased. Thus, we selected a high concentration of the TPA probe (665 mg L^{-1}) and only detected the TOF during the first 20 seconds. Nevertheless, the final measured and calculated values are still not the most accurate results, but the actual values are definitely greater than the calculated values. Therefore, it is reasonable to use this method to calculate the TOF to reflect the efficiency of •OH formation on the catalyst. In the first 20 s, the concentration of the generated •OH was measured as 7.44×10^{-5} mol L^{-1}, when the concentration of the catalyst [$\boldsymbol{C(catal.)}$] was 0.4 g L^{-1} and the initial concentration of H_2O_2 [$\boldsymbol{C(H_2O_2)}$] was 10 mM. The formation rate of •OH [$\boldsymbol{V(^{\bullet}OH)}$] was thus obtained from the above •OH quantification experiment within the first 20 s ($\boldsymbol{V(^{\bullet}OH)}$= 3.72×10^{-6} mol L^{-1} s^{-1}). The main active sites are the Cu centers, and their amount depends on the surface Cu concentration, which was determined by the Langmuir adsorption isotherms of phenol on the CuCo-Al_2O_3 matrix (before growing g-C_3N_4 on the surface) due to the strong complexing of Cu and phenol. In a typical procedure, 0.02 g of CuCo-Al_2O_3 was added into 50 mL of the phenol solution with phenol concentrations of 2, 5, 10, 20, 30, 50, 75, 100, and 150 mg L^{-1}. The suspensions were magnetically stirred throughout the experiment. At given time intervals, 3 mL aliquots were collected and filtered through a Millipore filter (pore size 0.45 μm) for analysis until the maximum adsorption amount of phenol was attained for each set of experiments. The concentrations of phenol were determined using a 1200 series HPLC (Agilent, U.S.A.) equipped with a ZORBAX Eclipse XDB-C_{18} column and a UV detector. The mobile phase consisted of a mixture of

methanol/water at a flow rate of 1 mL min^{-1}. The 9 maximum adsorption amount values were drawn into an adsorption curve of phenol and fitted via the Langmuir adsorption isotherm model, and then the equilibrium adsorption amount was obtained as $q_e = 7.14 \times 10^{-6}$ mol g^{-1}. Thus, the number [***N(surf.)***] of active sites on the surface of the catalyst was approximately 4.3×10^{18} g^{-1}. The TOF of OH-CCN/CuCo-Al_2O_3 can be calculated by the following equation (eq. S1):

$$TOF = V(^{\bullet}OH) \bullet N_A / [C(catal.) \bullet N(surf.)] = 1.3\ s^{-1} \quad (S1)$$

Calculation of the utilization efficiency of H_2O_2. The complete mineralization of one mole of benzene, phenol, benzoic acid, phloroglucinol, bisphenol A, 2-chlorophenol, 4-isopropylphenol, ibuprofen, phenytoin, diphenhydramine, 2,4-dichlorophenoxyacetic acid, methyl orange, rhodamine B, methylene blue and atrazine will theoretically consume 15, 14, 15, 12, 36, 13, 23, 33, 39, 46, 15, 43, 73, 51 and 35 moles of H_2O_2, respectively (eqs. S2~S16).

1. benzene:

$$C_6H_6+15H_2O_2 \rightarrow 6CO_2+18H_2O \quad (S2)$$

2. phenol:

$$C_6H_6O+14H_2O_2 \rightarrow 6CO_2+17H_2O \quad (S3)$$

3. benzoic acid:

$$C_7H_6O_2+15H_2O_2 \rightarrow 7CO_2+18H_2O \quad (S4)$$

4. phloroglucinol:

$$C_6H_{10}O_5+12H_2O_2 \rightarrow 6CO_2+17H_2O \quad (S5)$$

5. bisphenol A:

$$C_{15}H_{16}O_2+36H_2O_2 \rightarrow 15CO_2+44H_2O \quad (S6)$$

6. 2-chlorophenol:

$$C_6H_5OCl+13H_2O_2 \rightarrow 6CO_2+15H_2O+HCl \quad (S7)$$

7. 4-isopropylphenol:

$$C_9H_{12}O+23H_2O_2 \rightarrow 9CO_2+29H_2O \quad (S8)$$

8. ibuprofen:

$$C_{13}H_{18}O_2+33H_2O_2 \rightarrow 13CO_2+42H_2O \quad (S9)$$

9. phenytoin:

$$C_{15}H_{12}N_2O_2+39H_2O_2 \rightarrow 15CO_2+44H_2O+2HNO_3 \quad (S10)$$

10. diphenhydramine:

$$C_{17}H_{21}NO+46H_2O_2 \rightarrow 17CO_2+56H_2O+HNO_3 \quad (S11)$$

11. 2,4-dichlorophenoxyacetic acid:

$$C_8H_6Cl_2O_3+15H_2O_2 \rightarrow 8CO_2+17H_2O+2HCl \quad (S12)$$

12. methyl orange:

$$C_{14}H_{14}N_3SO_3Na+43H_2O_2 \rightarrow 14CO_2+48H_2O+2HNO_3+H_2SO_4+NaNO_3 \quad (S13)$$

13. rhodamine B:

$$C_{28}H_{31}ClN_2O_3+73H_2O_2 \rightarrow 28CO_2+87H_2O+HCl+2HNO_3 \quad (S14)$$

14. methylene blue:

$$C_{16}H_{18}ClN_3S+51H_2O_2 \rightarrow 16CO_2+57H_2O+HCl+3HNO_3+H_2SO_4 \quad (S15)$$

15. atrazine:

$$C_8H_{14}ClN_5+35H_2O_2 \rightarrow 8CO_2+39H_2O+HCl+5HNO_3 \quad (S16)$$

The utilization efficiency of H_2O_2 (η) is defined as the ratio of the stoichiometric H_2O_2 consumption ($[\Delta H_2O_2]_S$) for the mineralization of pollutants to the actual H_2O_2 consumption ($[\Delta H_2O_2]_A$) in the Fenton-like reaction[11] and is expressed in eq. S17:

$$\eta = [\Delta H_2O_2]_S / [\Delta H_2O_2]_A \quad (S17)$$

By measuring the TOC change in the pollutant solutions, the amounts of the mineralized contaminants were obtained, and the value of $[\Delta H_2O_2]_S$ was calculated. The actual H_2O_2 consumption ($[\Delta H_2O_2]_A$) at different reaction times was measured using the DPD method. The detailed data for $[\Delta H_2O_2]_A$ and $[\Delta H_2O_2]_S$ are presented in **Table S3**.

References

1 X. Zhang, Y. Ding, H. Tang, X. Han, L. Zhu and N. Wang, *Chem. Eng. J*., 2014, **236**, 251-262.

2 R. Huang, Z. Fang, X. Yan and W. Cheng, *Chem. Eng. J.*, 2012, **197**, 242-249.

3 N. Wang, L. Zhu, M. Lei, Y. She, M. Cao and H. Tang, *ACS Catal.*, 2011, **1**, 1193-1202.

4 X. Yang, P.-F. Tian, C. Zhang, Y.-Q. Deng, J. Xu, J. Gong and Y.-F. Han, *Appl. Catal. B: Environ.*, 2013, **134-135**, 145-152.

5 A. L. Ankudinov, B. Ravel, J. J. Rehr and S. D. Conradson, *Phys. Rev. B*, 1998, **58**, 7565-7576.

6 A. D. Becke, *J. Chem. Phys.*, 1993, **98**, 5648-5652

7 M. J. Frisch et al, *Gaussian09, Revision D.01*, Gaussian, Inc., Wallingford CT, 2009.

8 T. Lu and F. Chen, *J. Comput. Chem.*, 2012, **33**, 580-592.

9 W. Humphrey, A. Dalke and K. Schulten, *J. Mol. Graphics Modell.*, 1996, **14**, 33-38.

10 H. Bader, V. Sturzenegger and J. Hoigne, *Water Res.*, 1988, **22**, 1109-1115.

11 L. Lyu, L. Zhang, Q. Wang, Y. Nie and C. Hu, *Environ. Sci. Technol.*, 2015, **49**, 8639-8647.